RESEARCH ARTICLE

Application of Novel Design Bone Grafting for Treatment of Segmental Acetabular Rim Defects During Revision Total Hip Arthroplasty

Xin Zhao[1] · Haowen Xue[1] · Yang Sun[1] · Aobo Zhang[1] · Yang Liu[1] · Hao Chen[1] · Qian Wan[1] · Jiangbo Zhang[1] · Jianlin Xiao[2] · Chenyu Wang[3] · Qing Han[1] · Jincheng Wang[1]

Abstract

The study aimed to develop efficient techniques with different novel graft structures to enhance the treatment of acetabular bone deficiency. The inhomogeneous material properties Finite Element Analysis (FEA) model was reconstructed according to computed tomography images based on a healthy patient without any peri-acetabular bony defect according to the American Academy of Orthopedic Surgeons (AAOS). The FEA model of acetabular bone deficiency was performed to simulate and evaluate the mechanical performances of the grafts in different geometric structures, with the use of fixation implants (screws), along with the stress distribution and the relative micromotion of graft models. The stress distribution mainly concentrated on the region of contact of the screws and superolateral bone. Among the different structures, the mortise–tenone structure provided better relative micromotion, with suitable biomechanical property even without the use of screws. The novel grafting structures could provide sufficient biomechanical stability and bone remodeling, and the mortise–tenone structure is the optimal treatment option for acetabulum reconstruction.

1 Introduction

The treatment of acetabular bone deficiency represents a challenging issue in total hip arthroplasty [1, 2]. Various techniques for reconstructing large acetabular defects and pelvic discontinuity have been developed [3, 4]. Acetabulum defects are classified as segmental and cavitary defects according to the classification of the American Academy of Orthopedic Surgeons (AAOS) [5]. Large acetabular bone defects usually involve a combination of cavitary and segmental bone deficiencies that require various reconstruction strategies. The basic principles of acetabular defect reconstruction are to restore bone coverage and hip rotation center, preserve bone around the acetabulum and regain functional biomechanics, with aims for better stability and normal range of movement [6–9]. Several approaches have been identified to address the difficulty in acetabular reinforcement including bone grafts, reinforcement rings and cages [1, 10, 11].

Screw fixation is commonly used during acetabulum reconstruction. However, this technique is associated with complications, including screw fracture and pull-out, bone nonunion and resorption of the bone block [12, 13]. The mortise–tenone joint form design originates from ancient Chinese architecture and is a structure without a single screw; this joint form has been used for thousands of years [14, 15]. The mortise–tenone joint features a combination of interlocking features and remarkable stiffness. However, this

✉ Jianlin Xiao
  xiaojianlin10@jlu.edu.cn

✉ Chenyu Wang
  wangchenyu@jlu.edu.cn

✉ Qing Han
  my.hanqing@163.com

✉ Jincheng Wang
  jinchengwangjlu@163.com

1. Orthopaedic Medical Center, The 2nd Hospital of Jilin University, Changchun 130041, China

2. Department of Orthopaedics, China-Japan Union Hospital of Jilin University, Changchun 130033, China

3. Department of Plastic and Reconstructive Surgery, First Bethune Hospital of Jilin University, Changchun 130021, China

crosslink structure has not been reported as an orthopedic implant structural design scheme.

In this study, we developed an integrated method to investigate the biomechanical changes in peri-acetabular graft structures by employing the biomechanical parameters of FEA. We introduced four different graft structures: the circular, wedge, square and mortise–tenone structures. Finite Element Analysis (FEA) and biomechanical parameters such as stress distribution and relative micromotion were analyzed. We further examined the mortise–tenone-shaped FEA models with and without screws to evaluate the feasibility of the no-screw concept and reduce the number of screws at final implantation. In addition, we analyzed the optimal structure for reconstruction aimed at providing durable outcome.

2 Materials and Methods

The hip joint inhomogeneous FEA models used in this study can represent the geometric native hip model and differentiate cortical and cancellous bone. Four different bone graft models were designed based on the typical pelvic model: circular, wedge, square and mortise–tenone structures. Segmental acetabular rim defects were incorporated as seen in actual practice.

2.1 Bone Grafting Model Reconstruction and Surgical Simulation

Computed Tomography (CT) scan data were obtained from a healthy individual without any acetabular bone defect. The Philips iCT 256 CT scanner was used to obtain a slice thickness of 0.602 mm at 156 mA and 120 kVp. Mimics Research 21.0 (Materialise, Belgium) was used to create a pelvic three-dimensional (3D) model using the scan data. Region growing and contour interpolation method was applied to perform semi-automatic segmentation of the CT image data and identify the boundary of the hemipelvis. The radiographic density of CT images and corresponding Hounsfield Units (HU) were used to represent the material properties of the pelvic bone and graft bone. Mimics formulas from previous research were used, and the relationship of HU and bone density (ρ) (g·cm^{-3}) and Young's modulus (E) (MPa) in pelvic bone were assigned as follows [16]:

$$\rho = 1.9 \times 10^{-3} Hu + 0.105 \, Hu \leq 816 \tag{1}$$

$$\rho = 7.69 \times 10^{-4} Hu + 1.028 \, Hu > 816 \tag{2}$$

$$E = 2875\rho^3 \tag{3}$$

In this study, the material properties of graft bone were assigned as femoral bone, because femoral head graft is commonly used as bulk structural autograft or allograft. The relationship of HU and bone density (ρ) (g·cm^{-3}) and Young's modulus (E) (MPa) in graft bone were assigned as follows [17]:

$$\rho = -1.34 \times 10^{-5} Hu + 1.017 \times 10^{-3} \tag{4}$$

$$E = -0.3888 + 5.925\rho \tag{5}$$

The inhomogeneous FEA models were divided into ten materials on the premise of the ten HU values in the acetabular bone deficiency models and the graft bone models. For cortical and cancellous bone, a density–elastic modulus relationship was used to assign material properties for each element, which was divided into ten colors. The Poisson's ratio of all models was assigned as 0.30. A schematic plot and the properties are shown in Fig. 1.

A type I segmental defect occurring in the superior half portion of the acetabulum including the anterior column, superior aspect, and posterior column along the acetabular rim was generated to fit the AAOS classification. One acetabular bone deficiency model and four different operation models and their corresponding graft bone models were designed and reconstructed based on a normal integrated pelvis 3D model using Magics 24.0 (Materialise, Belgium). To better simulate the force state of the acetabulum, a simplified model of an acetabular cup with the femoral head was designed as a hemispherical structure. A 60-mm diameter sphere was used to cut the pelvic bone to design and simulate acetabulum and acetabular cup after surgery. The acetabular cup diameter and the bearing surface diameter of the simplified model of the femoral head were 60 mm. The acetabular bone deficiency model was constructed using another 60-mm diameter sphere; the medial edge of the deficiency was re-constructed on the perpendicular line from the center of the head. The circle-shaped grafting bone was fit to the structure of the acetabular bone deficiency to reconstruct the integrated pelvis. The other models of the grafting bone were cut diagonally along the shape of the edge of the defect at an incline and vertical angle on the sagittal sectional image. At the medial edge of the defect, the square and mortise–tenone-shaped grafting bone models were cut perpendicularly, and a 45-degree operative incline was applied in the wedge model. At the top edge of the defect, a horizontal cutting method was used in the wedge and square models and a horizontal dip angle of 30-degree cutting method was used to construct the mortise–tenone. In the sagittal plane, the rectangular model of grafting bone was cut perpendicularly along the edge of the defect. The height, width, and depth of the grafting bone were 43.00 mm, 53.00 mm, 25.81 mm in the circle model
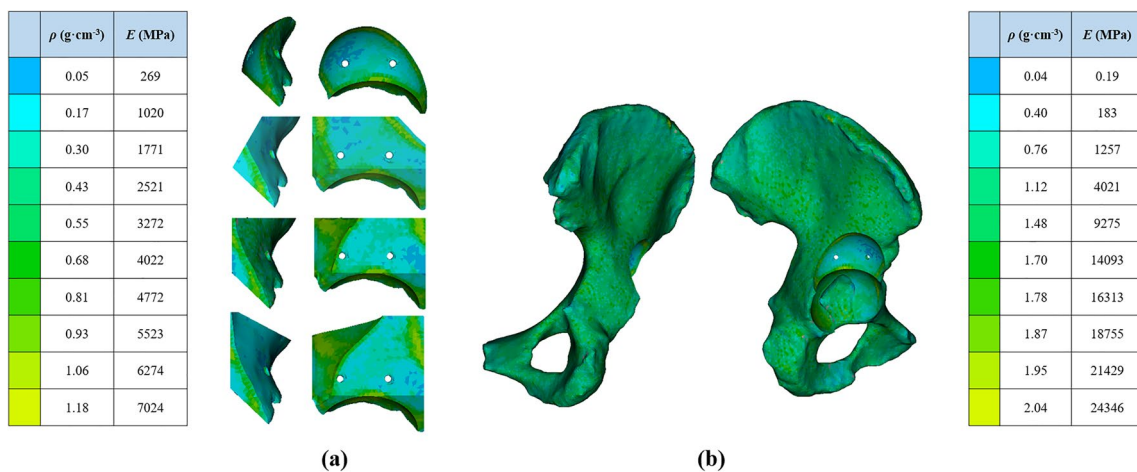
Fig. 1 The elasticity modulus distribution of grafting bone and pelvic FEA model based on Hounsfield units of CT data. **a** The model of grafting bone; **b** the model of the pelvis. ρ represents bone density; *E* represents elasticity modulus

(Fig. 2a), 43.00 mm, 53.00 mm, 32.43 mm in the wedge model (Fig. 2b), 43.00 mm, 53.00 mm, 30.59 mm in the square model (Fig. 2c) and 55.30 mm, 53.00 mm, 28.89 mm in the mortise–tenone model (Fig. 2d). The cup was placed in the recovery structure consisting of the acetabulum and graft with lateral and anterior angles of 45 degrees and 15 degrees. For the models with screws, two cancellous screws were used to hold the graft in position. A 30-mm and a 35-mm cancellous screw were advanced to penetrate through the appropriate site of bone grafting and the cortical bone of pelvis. All of the diameters of the screws were 5 mm. The 35-mm screw and 30-mm screw were placed in the lateral and medial pelvis, respectively. The elasticity modulus and Poisson's ratio of the simplified femoral head model were

set to 17,000 Mpa and 0.3, respectively. Each graft model was fixed by two cortical screws with an elasticity modulus of 110,000 Mpa and a Poisson's ratio of 0.3.

2.2 Boundary and Loading Conditions

The resulting model, in stl and inp file format, was imported into HyperMesh 2020 (Altair, USA). The triangle-based surface meshes in pelvis and graft models were set as 2 mm using the automatic mesh technique. Because of the small screw thread features, the size of screw meshes was 1 mm. Volume meshes were made as tetrahedral elements after 2D meshing (Table 1). The friction types of each contact surface were determined according to the data from our previous
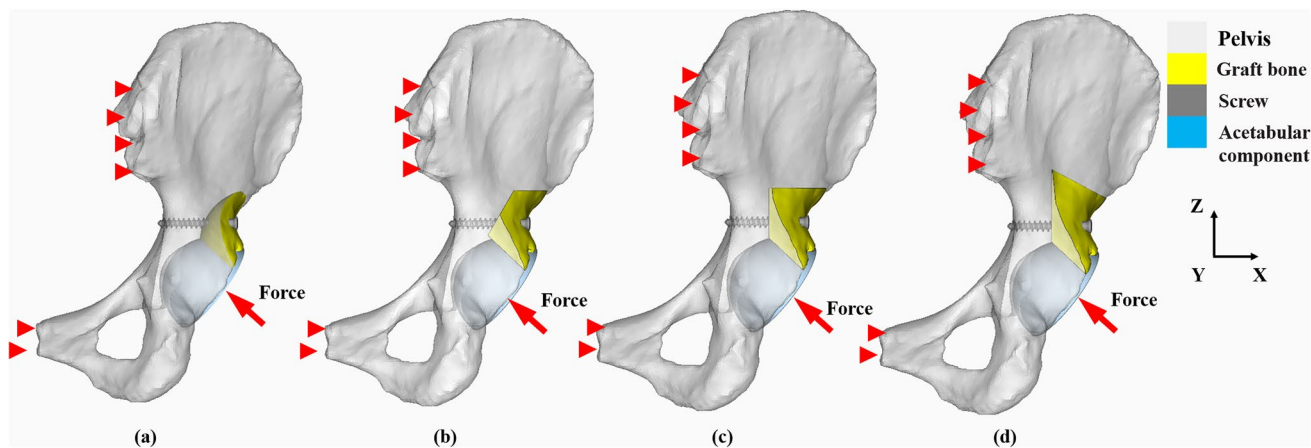

Fig. 2 The components and loading conditions of the four FEA models. **a** The model of the circle joint acetabular defect; **b** the model of the wedge joint acetabular defect; **c** the model of the square joint acetabular defect; **d** the model of the mortise–tenone joint acetabular defect. The 35-mm screw was placed in the lateral pelvis and 30-mm screw was placed medially. Arrowheads and triangles indicate the loads and constraint of FEA models, respectively

Table 1 The parameters of the FE model

Component	Material type	Element	Element type
Circle shaped	Pelvis	221,274	Inhomogeneous
	Graft bone	29,468	
Wedge shaped	Pelvis	213,248	
	Graft bone	38,514	
Square shaped	Pelvis	206,694	
	Graft bone	45,580	
Mortise–tenone shaped	Pelvis	209,184	
	Graft bone	46,826	
35 mm screw	Ti-6Al-4 V	14,228	Homogeneous
30 mm screw	Ti-6Al-4 V	7976	
Acetabular component	Cortical bone	26,890	

Table 2 Friction types between components

Contact surface A	Contact surface B	Friction type
Pelvis	Acetabular cup	Static friction ($\mu = 0.1$)
Pelvis	Graft bone	Static friction ($\mu = 0.88$)
Pelvis	Screw	Stick
Graft bone	Screw	Stick

study [18] and the surface of contact was considered to behave as a nonlinear contact surface (Table 2). The load condition of the static analysis performed in this study was the same as that applied by Bergmann et al. [19]. The peak load for the unilateral hip joint was 1948 N for the normal gait of individuals who undergo total hip arthroplasty. Sacroiliac joint and pubic symphysis were assumed as fixed constraint boundaries (Fig. 2) [18]. Quasi-static loading nonlinear analysis was employed in the simulation procedure with iterate 20 steps until convergence, and the iterative method was performed using the Newton–Raphson method. The stress distribution and relative micromotion were selected as main parameters to verify the effect of stress shielding and the effect of bone growth. The results were obtained and measured in HyperView (Altair, USA).

3 Results and Discussion

Revision total hip arthroplasty in patients with large acetabular bone defects is a clinical problem on account of the loss of acetabular bone stock, and therefore bone grafting is required for acetabular augmentation [2, 20]. Defects of the acetabulum in complex primary hips are generally caused by late presentation in inflammatory arthritis, postoperative bone tumor surgery, developmental dysplasia of the hip or posttraumatic sequelae [21, 22]. Many techniques have been described to address bone defects. Autografts and allografts

prepared from resected femoral head are widely applied [23]. The clinical results of impaction bone grafts in the acetabulum have been reported, and survival varies from 84% at 8 years to 52% at 25 years [24, 25]. This method has been accepted because it restores bone stock in preparation for future revision surgery and provides support in a better anatomic position. However, numerous cases of failure due to complications such as graft resorption, collapse, and socket have been reported [25, 26]. The use of bulk graft has thus been controversial. Some studies have indicated that the size of the bone defect is an important factor contributing to failure [27, 28]. There is no standard technique for reconstruction to restore normal hip biomechanics. Therefore, the purpose of our study was to design a suitable graft structure for repairing acetabular defects. We evaluated mechanical performance of grafts using FEA software.

According to Wolff's law, after failure of structural bone grafting, bone tissues are absorbed and result in collapse. A higher risk of structural bone graft failure is present if the coverage of the cup is less than 50% [10].

Few studies have analyzed the biomechanical FEA of the pelvis following defect repair. Fu et al. reconstructed an integrated acetabular bone defect and FEA model by the 3D printed Ti_6Al_4V augment and trabecular metal augment [29] and Amirouche et al. analyzed cup insertion and fixation in the context of various segmental acetabular defects [1]. Levine et al. presented an FEA study of revision total hip arthroplasty to explore the influence of defect size and shape on periprosthetic bone stress, and trabecular metal implants were selected to fill the defects [30]. A simple bone defect and metal augment were used in these studies. However, no FEA study has been performed for structural optimization and biomechanics analysis of graft bone.

3.1 Comparison of Stress Results Among the Four Structures

This study focused on the stress distribution of postoperative acetabular bone, graft bone and screws for fixing implants and examined whether they were greater than the yield strength of the corresponding materials. Stresses are generated in implant and bone and at their interface. Mechanical stress is an essential factor to support bone tissue remodeling, but excessive load is one of the main inducers of fatigue damage [7]. Therefore, it is important for acetabular bone and graft bone to attain a proper state of stress distribution. By comparing the results from the FEA models shown in Fig. 3, the von Mises stress distribution was observed to increase on the upside interface of both the pelvis and graft bone with the square and mortise–tenone implant. These findings showed that implants were in contact with the superolateral region of the acetabular cup and had a greater stress distribution, which would undergo remodeling from
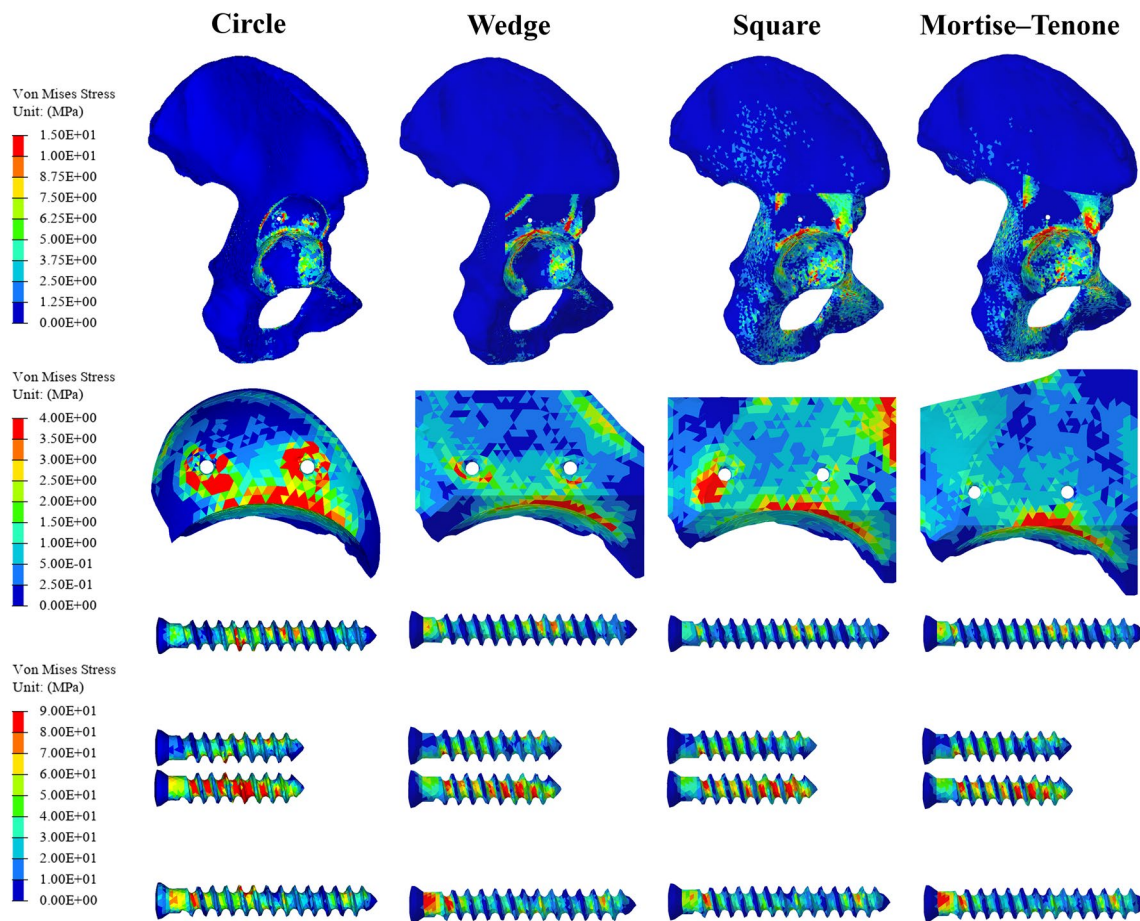
Fig. 3 Comparison of the stress distribution of different acetabular defects. Three components including pelvis, graft bone and screws were compared; the 35-mm screw and 30-mm screw were placed laterally and medially, respectively

sufficient stress stimulation from the main loading region [7]. These results indicate that the design of the square and mortise–tenone structures are acceptable according to the stress results. We observed one difference among the structures. The maximum principal stress in the mortise–tenone pelvis (34.74 MPa) and graft models (7.53 MPa) was lower than the fatigue strength of the cortical bone (37–57 MPa) (Fig. 4) [31]. Nevertheless, the values measured from the pelvis in the circle-shaped (45.66 MPa), wedge-shaped (37.82 MPa) and square-shaped models (46.83 MPa) were all greater than the lower limit of the fatigue strength. Early fatigue failure would occur in the postoperative period under the condition of contact stress emerging around the screw hole at the superolateral compartment in all structures except the mortise–tenone type bone block. Thus, the mortise–tenone-shaped implant may be a more suitable treatment design for large acetabular bone deficiency.

Cortical screw fracture and pull-out are common complications after acetabular reconstruction. We examined the stress distribution and values on screws in each group (Fig. 3); the stress distribution on screws showed that stress
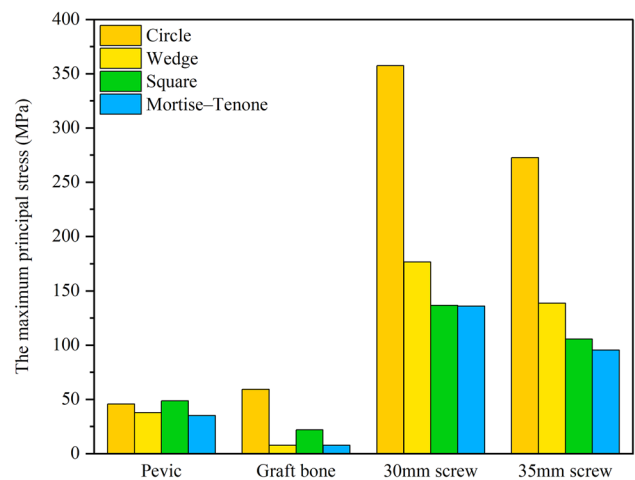

Fig. 4 The maximum principal stress in the four types of acetabular defects

concentrated at the bottom junction part with graft bone. Figure 4 shows the maximum principal stress value in different

components. A significantly large value (357.49 MPa) at the screw was observed in the circle-shaped model. The maximum Von Mises peak stress values were 59.17 MPa, 357.49 MPa and 272.54 MPa for the graft bone, 30 mm screw and 35 mm screw in the circle-shaped bone defect component, respectively. In these four groups, the maximum principal stress values were all lower than the yield strength of Ti-6Al-4 V alloy (789–1013 MPa) [31], which indicated that the strength of the screws can sustain the static loading requirement. In addition, the long-term survival of the screws needs to take into account that the maximum stress should be far below the fatigue strength limitation of the titanium alloy (310–610 MPa) [32]. As the circular structure of bone graft may not provide a better lateral stiffness than other structures, the screws in this model have great stress values (357.49 MPa, 275.54 MPa), which are even greater than the fatigue strength. The circular grafting structure is generally used in routine treatment. Therefore, these results indicate that traditional acetabular reconstruction techniques show a risk of screw-related complications.

3.2 Comparison of Relative Micromotion Results Among the Four Structures

To examine the mechanism of stability and the relationship of bone formation in different structures, the relative micromotion ratio was calculated by counting the percentage of the points with micromotion less than 28 µm in the selected region at the intersection of pelvis and graft bone. The function of the selected points in the overall and side edge are shown in in Fig. 5. Previous studies showed that a micromotion of > 150 µm leads to fibrous tissue formation, while adequate osseous contact and fixation minimizes micromotion and prevents fibrous ingrowth; micromotion between 30 and 150 µm leads to bone and fibrous tissue formation; and micromotion < 28 µm results in predominant bone formation [8, 9]. Our results showed that the mortise–tenone structure had a larger ratio value and a smaller ratio value

was observed in the circle structure. In addition, the maximum micromotions in the circle, wedge, square and mortise–tenone-shaped bone defect models were 81 µm, 143 µm, 121 µm and 123 µm, respectively, all at the lower inner quadrant. The relative micromotion ratio results showed micromotion less than 28 µm of the total ratio was 50%, 49.11%, 45.28%, and 40.91% in the mortise–tenone, square, wedge and circle structures, respectively (Fig. 6). Based on the results shown in Figs. 5 and 6, the regions of the relative micromotion < 28 µm mainly in the upper part of contact region. Hence, increasing the contact area of the upper part could provide more contact region that the relative micromotion < 28 µm, then may better decrease the micromotion of the interface and further improve the performance of bone formation. This demonstrated that the grafting structure of mortise–tenone could effectively prevent micromotion, promote bone remodeling and relieve postoperative pain caused by interfacial displacement.
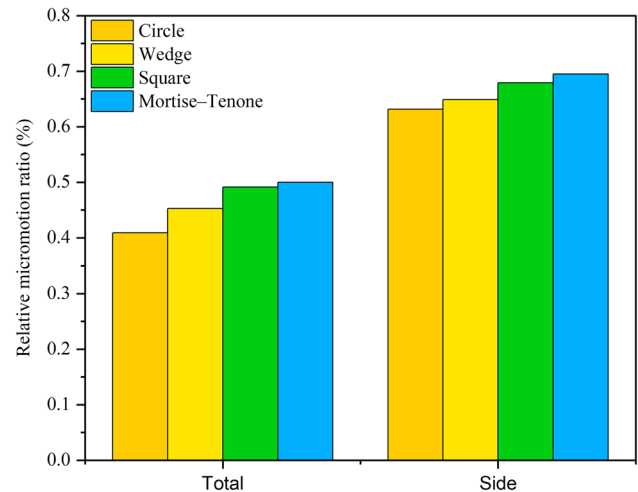

Fig. 6 The relative micromotion ratio in the four types of acetabular defects

Fig. 5 The relative micromotion of the four FEA models. The red and blue dotted lines indicate the location for the measurement of relative micromotion between the pelvis and grafting bone. Red dotted lines indicate the regions of relative micromotion < 28 µm. Blue dotted lines indicate the regions of relative micromotion > 28 µm. Arrowheads indicate the points of the maximum micromotions in FEA models
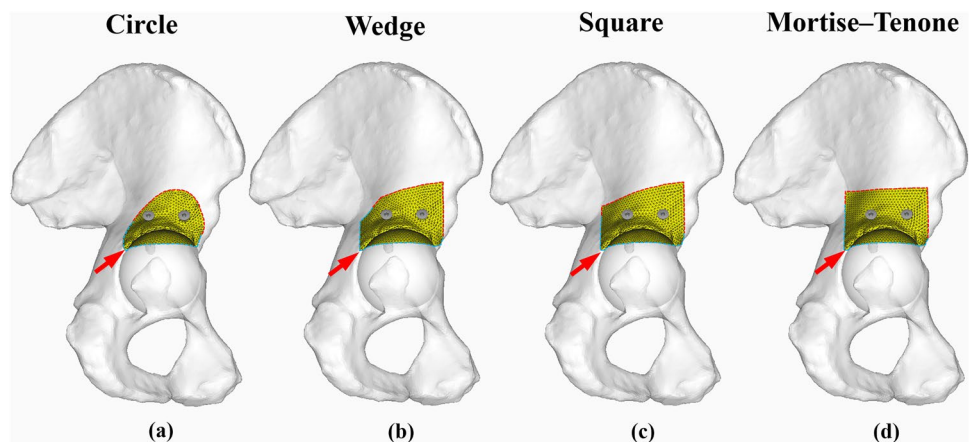
3.3 Comparison of Models with and Without Screws in the Mortise–Tenon Joint Structures

Mortise–tenon joint structures are widely seen in ancient timber structures in China [15]. The mechanical behavior of mortise–tenon joints is complex and their structural superiority could play an important role in the lateral and rotational stiffness, integrality and stability of the whole structure [15]. To verify the superiority of this structure, the screw was removed to present the integral grafting bone. The FEA results in Fig. 7a showed that the structure without screws has a wider stress distribution range in superior and medial parts. The relative micromotion ratio gradually decreases with the stress distribution range increasing in the same parts (Fig. 7b). When the screws are inserted into the components, the maximum principal stress reduces significantly, leading to prosthesis stability. In comparing the models with and without screws, more stress distribution was found concentrated at the superolateral region of grafting bone and greater stress (49.39 MPa) recorded at the cortical bone of pelvis (Fig. 7c), which has a greater probability of fatigue damage [31]. A possible explanation for this might be the effective stress borne by screws. The micromotion results indicated that the model without screws had 3more stable regions such as in inferior and lateral locations. Therefore, the implants of acetabular reconstruction without screws also could provide enough biomechanical property to stimulate bone remodeling and to increase stability. An increase in the number of screws could improve these indicators related to biomechanical characteristics [33]. Overall, this evidence supports the ability of absorbable inner fixation screws, so far as to no-screw applied, in the process of acetabular reconstruction.

Our previous findings suggest that novel designed grafting structure may be beneficial to acetabular bone defect patients, and thus the primary goal of structure optimization is to reduce postoperative complications, decrease the number of screws used for fixation, and provide a reference for clinical practice. Compared with the novel bone grafting design, the classical circular bone grafting design was not up to biomechanics characteristics. A striking finding from this study is that traditional mortise–tenon joint structures show biomechanical superiority and promote better results in terms of stress distribution and relative micromotion.

There are a few limitations in this study. First, characteristics specific to patients (bone density, dynamic biomechanical properties and surrounding soft tissue) were not addressed and the clinical behavior observed in an individual during surgery may not correspond to simulated conditions. In addition, we only analyzed type 1 AAOS rim defects, and future analyses to investigate other AAOS defect types and more complicated forms of acetabular bone loss are warranted.

4 Conclusion

This FEA-based study was conducted to provide insights into the reconstruction of acetabular bone defects during total hip arthroplasty revision. The effects of acetabulum reconstruction on stress distributions and relative micromotion in the contact surface of the acetabulum and grafting bone were investigated. Our results demonstrated that the mortise–tenone structure decrease micromotion and provided better stress distributions. With sufficient biomechanical stability and bone remodeling, the mortise–tenone graft structure is recommended for acetabulum segmental defect reconstruction. This design can reduce the complications of bone fracture, screw fracture and pull-out as well as osteolysis, among other complications. Our results provide references for clinical practice and a foundation for subsequent application in orthopedic surgery.
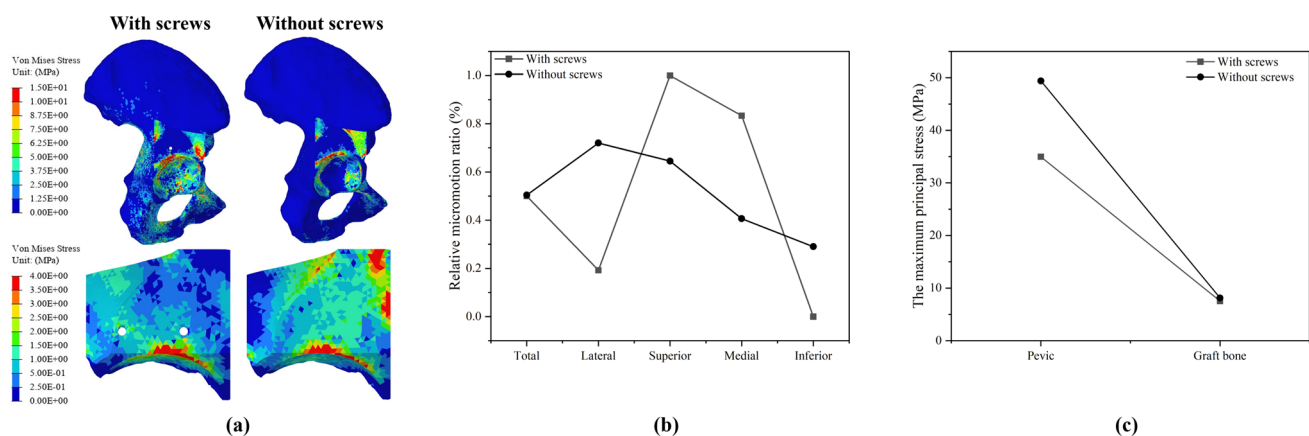

Fig. 7 Comparison of the mortise–tenone joint acetabular defects between the models with and without screws. **a** The results of the stress distribution; **b** the results of the relative micromotion ratio; **c** the results of the maximum principal stress

Declarations

Conflict of interest The authors declare they have no conflict of interest.

References

1. Amirouche, F., Solitro, G. F., Walia, A., Gonzalez, M., & Bobko, A. (2017). Segmental acetabular rim defects, bone loss, oversizing, and press fit cup in total hip arthroplasty evaluated with a probabilistic finite element analysis. *International Orthopaedics, 41*, 1527–1533.

2. Rodriguez, J. A., Huk, O. L., Pellicci, P. M., & Wilson, P. D. (1995). Autogenous bone grafts from the femoral head for the treatment of acetabular deficiency in primary total hip arthroplasty with cement. Long-term results. *Journal of Bone and Joint Surgery-American, 77*, 1227–1233.

3. Meynen, A., Matthews, H., Nauwelaers, N., Claes, P., Mulier, M., & Scheys, L. (2020). Accurate reconstructions of pelvic defects and discontinuities using statistical shape models. *Computer Methods in Biomechanics and Biomedical Engineering, 23*, 1026–1033.

4. Amenabar, T., Rahman, W. A., Hetaimish, B. M., Kuzyk, P. R., Safir, O. A., & Gross, A. E. (2016). Promising mid-term results with a cup-cage construct for large acetabular defects and pelvic discontinuity. *Clinical Orthopaedics and Related Research, 474*, 408–414.

5. D'Antonio, J. A., Capello, W. N., Borden, L. S., Bargar, W. L., Bierbaum, B. F., Boettcher, W. G., Steinberg, M. E., Stulberg, S. D., & Wedge, J. H. (1989). Classification and management of acetabular abnormalities in total hip arthroplasty. *Clinical Orthopaedics and Related Research, 243*, 126–137.

6. Atilla, B., Ali, H., Aksoy, M. C., Caglar, O., Tokgozoglu, A. M., & Alpaslan, M. (2007). Position of the acetabular component determines the fate of femoral head autografts in total hip replacement for acetabular dysplasia. *Journal of Bone and Joint Surgery-British, 89*, 874–878.

7. Mao, Y. Q., Yu, D. G., Xu, C., Liu, F. X., Li, H. W., & Zhu, Z. A. (2014). The fate of osteophytes in the superolateral region of the acetabulum after total hip arthroplasty. *Journal of Arthroplasty, 29*, 2262–2266.

8. Pilliar, R. M., Lee, J. M., & Maniatopoulos, C. (1986). Observations on the effect of movement on bone ingrowth into porous-surfaced implants. *Clinical Orthopaedics and Related Research, 208*, 108–113.

9. Jasty, M., Bragdon, C., Burke, D., O'Connor, D., Lowenstein, J., & Harris, W. H. (1997). In vivo skeletal responses to porous-surfaced implants subjected to small induced motions. *Journal of Bone and Joint Surgery-American, 79*, 707–714.

10. Du, Y., Fu, J., Sun, J., Zhang, G., Chen, J., Ni, M., & Zhou, Y. (2020). Acetabular bone defect in total hip arthroplasty for crowe II or III developmental dysplasia of the hip: a finite element study. *Biomed Research International, 2020*, 4809013.

11. Garala, K., Boutefnouchet, T., Amblawaner, R., & Lawrence, T. (2020). Acetabular reconstruction using a composite layer of impacted cancellous allograft bone and cement: minimum 5-year follow-up study. *Hip International*. https://doi.org/10.1177/1120700020941407

12. Samsami, S., Augat, P., & Rouhi, G. (2019). Stability of femoral neck fracture fixation: a finite element analysis. *Proceedings of the Institution of Mechanical Engineers, Part H: Journal of Engineering in Medicine, 233*, 892–900.

13. Park, J. Y., Kwon, H. M., Lee, W. S., Yang, I. H., & Park, K. K. (2021). Anthropometric measurement about the safe zone for transacetabular screw placement in total hip arthroplasty in asian middle-aged women: in vivo three-dimensional model analysis. *Journal of Arthroplasty, 36*, 744–751.

14. Shao, Z. X., Song, Q. F., Cheng, X., Luo, H., Lin, L., Zhao, Y. Q., & Cui, G. Q. (2020). An arthroscopic "Inlay" bristow procedure with suture button fixation for the treatment of recurrent anterior glenohumeral instability: 3-year follow-up. *American Journal of Sports Medicine, 48*, 2638–2649.

15. Chen, C. C., Qiu, H. X., & Lu, Y. (2016). Flexural behaviour of timber dovetail mortise-tenon joints. *Construction and Building Materials, 112*, 366–377.

16. Hao, Z. X., Wan, C., Gao, X. F., & Ji, T. (2011). The effect of boundary condition on the biomechanics of a human pelvic joint under an axial compressive load: A three-dimensional finite element model. *Journal of Biomechanical Engineering-Transactions of the Asme, 133*, 9.

17. Zhang, A. B., Chen, H., Liu, Y., Wu, N. C., Chen, B. P., Zhao, X., Han, Q., & Wang, J. C. (2021). Customized reconstructive prosthesis design based on topological optimization to treat severe proximal tibia defect. *Bio-Design and Manufacturing, 4*, 87–99.

18. Xiao, J. L., Zhao, X., Wang, Y. M., Yang, Y. H., Zhao, J. H., Gao, Z. L., & Zuo, J. L. (2018). Application of acetabular reinforcement ring with hook for correction of segmental acetabular rim defects during total hip arthroplasty revision. *Journal of Bionic Engineering, 15*, 154–159.

19. Bergmann, G., Deuretzbacher, G., Heller, M., Graichen, F., Rohlmann, A., Strauss, J., & Duda, G. N. (2001). Hip contact forces and gait patterns from routine activities. *Journal of Biomechanics, 34*, 859–871.

20. Pagnano, W., Hanssen, A. D., Lewallen, D. G., & Shaughnessy, W. J. (1996). The effect of superior placement of the acetabular component on the rate of loosening after total hip arthroplasty. *Journal of Bone and Joint Surgery-American, 78*, 1004–1014.

21. Mou, P., Liao, K., Chen, H. L., & Yang, J. (2020). Controlled fracture of the medial wall versus structural autograft with bulk femoral head to increase cup coverage by host bone for total hip arthroplasty in osteoarthritis secondary to developmental dysplasia of the hip: a retrospective cohort study. *Journal of Orthopaedic Surgery and Research, 15*, 12.

22. Muramatsu, K., Ihara, K., Hashimoto, T., Seto, S., & Taguchi, T. (2007). Combined use of free vascularised bone graft and extra-corporeally-irradiated autograft for the reconstruction of massive bone defects after resection of malignant tumour. *Journal of Plastic Reconstructive and Aesthetic Surgery, 60*, 1013–1018.

23. Goto, E., Umeda, H., Otsubo, M., & Teranishi, T. (2021). Cemented acetabular component with femoral neck autograft for acetabular reconstruction in Crowe type III dislocated hips a 20-to 30-year follow-up study. *Bone & Joint Journal, 103B*, 299–304.

24. Garcia-Cimbrelo, E., Cruz-Pardos, A., Garcia-Rey, E., & Ortega-Chamarro, J. (2010). The survival and fate of acetabular reconstruction with impaction grafting for large defects. *Clinical Orthopaedics and Related Research, 468*, 3304–3313.

25. Busch, V., Gardeniers, J. W. M., Verdonschot, N., Slooff, T., & Schreurs, B. W. (2011). Acetabular reconstruction with impaction bone-grafting and a cemented cup in patients younger than fifty years old a concise follow-up, at twenty to twenty-eight years, of a previous report. *Journal of Bone and Joint Surgery-American, 93A*, 367–371.

26. Gerber, S. D., & Harris, W. H. (1986). Femoral head autografting to augment acetabular deficiency in patients requiring total hip replacement. A minimum five-year and an average seven-year follow-up study. *Journal of Bone and Joint Surgery-American, 68*, 1241–1248.

27. van Haaren, E. H., Heyligers, I. C., Alexander, F. G. M., & Wuisman, P. (2007). High rate of failure of impaction grafting in large acetabular defects. *Journal of Bone and Joint Surgery-British, 89B*, 296–300.

28. Nelissen, R., Valstar, E. R., Poll, R. G., Garling, E. H., & Brand, R. (2002). Factors associated with excessive migration in bone impaction hip revision surgery—a radiostereometric analysis study. *Journal of Arthroplasty, 17*, 826–833.

29. Fu, J., Ni, M., Chen, J. Y., Li, X., Chai, W., Hao, L. B., Zhang, G. Q., & Zhou, Y. G. (2018). Reconstruction of severe acetabular bone defect with 3D printed Ti6Al4V augment: a finite element study. *Biomed Research International, 2018*, 6367203.

30. Levine, D. L., Dharia, M. A., Siggelkow, E., Crowninshield, R. D., Degroff, D. A., & Wentz, D. H. (2010). Repair of periprosthetic pelvis defects with porous metal implants: A finite element study. *Journal of Biomechanical Engineering-Transactions of the Asme, 132*, 021006.

31. Dong, E. C., Wang, L., Iqbal, T., Li, D. C., Liu, Y. X., He, J. K., Zhao, B. H., & Li, Y. (2018). Finite element analysis of the pelvis after customized prosthesis reconstruction. *Journal of Bionic Engineering, 15*, 443–451.

32. Long, M., & Rack, H. J. (1998). Titanium alloys in total joint replacement—a materials science perspective. *Biomaterials, 19*, 1627–1639.

33. Zhao, X., Chosa, E., Yamako, G., Watanabe, S., Deng, G., & Totoribe, K. (2013). Effect of acetabular reinforcement ring with hook for acetabular dysplasia clarified by three-dimensional finite element analysis. *Journal of Arthroplasty, 28*, 1765–1769.